A synthesis of global particle export from the surface ocean and cycling through the ocean interior and on the seafloor

John P. Dunne,[1] Jorge L. Sarmiento,[2] and Anand Gnanadesikan[1]

Received 30 November 2006; revised 29 May 2007; accepted 12 July 2007; published 19 October 2007.

[1] We present a new synthesis of the oceanic cycles of organic carbon, silicon, and calcium carbonate. Our calculations are based on a series of algorithms starting with satellite-based primary production and continuing with conversion of primary production to sinking particle flux, penetration of particle flux to the deep sea, and accumulation in sediments. Regional and global budgets from this synthesis highlight the potential importance of shelves and near-shelf regions for carbon burial. While a high degree of uncertainty remains, this analysis suggests that shelves, less than 50 m water depths accounting for 2% of the total ocean area, may account for 48% of the global flux of organic carbon to the seafloor. Our estimates of organic carbon and nitrogen flux are in generally good agreement with previous work while our estimates for $CaCO_3$ and SiO_2 fluxes are lower than recent work. Interannual variability in particle export fluxes is found to be relatively small compared to intra-annual variability over large domains with the single exception of the dominating role of El Niño-Southern Oscillation variability in the central tropical Pacific. Comparison with available sediment-based syntheses of benthic remineralization and burial support the recent theory of mineral protection of organic carbon flux through the deep ocean, pointing to lithogenic material as an important carrier phase of organic carbon to the deep seafloor. This work suggests that models which exclude the role of lithogenic material would underestimate the penetration of POC to the deep seafloor by approximately 16–51% globally, and by a much larger fraction in areas with low productivity. Interestingly, atmospheric dust can only account for 31% of the total lithogenic flux and 42% of the lithogenically associated POC flux, implying that a majority of this material is riverine or directly erosional in origin.

Citation: Dunne, J. P., J. L. Sarmiento, and A. Gnanadesikan (2007), A synthesis of global particle export from the surface ocean and cycling through the ocean interior and on the seafloor, *Global Biogeochem. Cycles*, *21*, GB4006, doi:10.1029/2006GB002907.

1. Introduction

[2] The sinking flux of particles from the surface ocean is a central driver of ocean biogeochemical cycling. Description of this flux and its fate within the water column is critical to understanding the global cycling of the elements. A number of attempts have been made to assess this flux on the global scale, both surface-down estimates using satellite color [*Laws et al.*, 2000] and seafloor-up estimates using benthic oxygen fluxes [*Jahnke*, 1996]. The first type of synthesis from the surface down requires a series of algorithms: first, to estimate satellite chlorophyll from observed radiances [e.g., *Feldman et al.*, 1989], second, to estimate primary production from this observed chlorophyll [*Ryther and Yentsch*, 1957; *Platt*, 1986; *Behrenfeld and Falkowski*, 1997], third, to estimate the fraction of primary production that is exported [*Laws et al.*, 2000], fourth, to estimate the depth-dependence of remineralization of the exported organic carbon [e.g., *Martin et al.*, 1987; *Klaas and Archer*, 2002], and finally, to estimate the fate of the carbon that reaches the ocean bottom. In order to utilize a mineral protection scheme in our analysis, we also require estimates of biogenic opal and calcium carbonate and lithogenic material in sinking fluxes and estimates of the degree to which their remineralization or dissolution profiles within the water column and the sediments differ from organic carbon [e.g., *Berelson*, 2002].

[3] Extensive work over the past few years has addressed some of the systematic biases associated with earlier estimates. New estimates of chlorophyll distribution have been developed to correct previous biases [*Gregg et al.*, 2002]; and a suite of algorithms have been developed to estimate primary production from satellite-inferred chlorophyll and subsequently compared in the Primary Production Algorithm Round-Robin series [e.g., *Campbell et al.*, 2003, and references therein]. Attempts have also been made to utilize the growing database of biogeochemical field process studies to more comprehensively establish both the relationship of particle export with primary production [*Dunne*

[1]NOAA Geophysical Fluid Dynamics Laboratory, Princeton, New Jersey, USA.
[2]Atmospheric and Oceanic Sciences Program, Princeton University, Princeton, New Jersey, USA.

0886-6236/07/2006GB002907$12.00

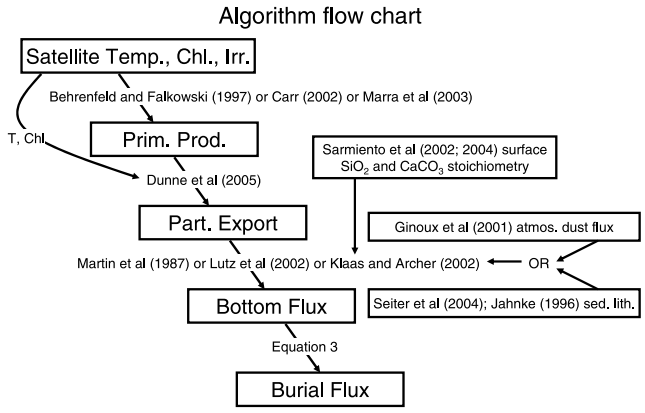

Figure 1. Flow diagram of analysis method starting with satellite estimates.

et al., 2005], and the attenuation of particles to the deep sea [*Lutz et al.*, 2002]. In addition, recent estimates of the stoichiometry of nutrient removal [*Sarmiento et al.*, 2002, 2004; this work] in surface waters allows extension of global organic carbon fluxes to the fluxes of SiO_2, $CaCO_3$, and lithogenic material.

[4] For the first time, this suite of algorithms affords not only a means to synthesize a more complete biogeochemical budget than previously available but also to estimate the variability and uncertainty in these biogeochemical fluxes. Our approach is to combine a suite of previously introduced algorithms to relate satellite observations to fluxes through the water column and the sediments. At each step, we assess the temporal and geographical variability and accumulating uncertainty in the estimates. The comprehensive nature of this summary provides a previously unavailable assessment of the global carbon budget fully independent of general circulation model results, making it an important point of comparison in the development of earth system models of ocean biogeochemical cycles in atmospheric CO_2 variability.

2. Methods

2.1. Data Sources

[5] In this section, we describe the input data and flux algorithms used here and present a flow diagram of this analysis method in Figure 1. Because many of these algorithms are nonlinear with respect to their input parameters, we have attempted to minimize temporal biases accrued during averaging in the propagation of flux estimates through the various algorithms by performing all calculations on the time-varying fields of chlorophyll, temperature and irradiance rather than on climatologies of these fields. All data sets were interpolated onto the uniform one-degree Levitus grid in order to provide a consistent and computationally manageable framework for calculations. We include all the marginal seas except the Caspian Sea. We utilized satellite chlorophyll and photosynthetically active radiation (PAR) from SeaWiFS monthly 9 km composite fields from 1998–2004 courtesy of the Goddard Earth Sciences Distributed Active Archive Center (http://disc.sci.gsfc.nasa.gov/guides/GSFC/guide/SeaWiFS_L3_Guide.gd.shtml) and monthly fields of surface temperature and irradiance from the NCEP reanalysis courtesy of the NOAA-NCEP-NCAR Climate Data Assimilation System I Reanalysis Project [*Kalnay et al.*, 1996] (http://iridl.ldeo.columbia.edu/SOURCES/.NOAA/.NCEP-NCAR/.CDAS-1/.MONTHLY/.Diagnostic/.surface/). Nutrient data were taken from the World Ocean Atlas 2001 Database (http://www.nodc.noaa.gov/OC5/WOA01/pr_woa01.html). While higher temporal (8 d) and spatial (1 km) resolution data sets were available, their usefulness was limited by clouds.

2.2. Primary Production

[6] We estimate primary productivity from chlorophyll, temperature and PAR using algorithms of *Behrenfeld and Falkowski* [1997] (algorithm available at http://www.marine.rutgers.edu/opp/programs/VGPM.html), *Carr* [2002] (algorithm kindly provided by personal communication), and *Marra et al.* [2003] (algorithm kindly provided by personal communication) to develop a range of uncertainty between these estimates. A more rigorous assessment of the uncertainty is currently being carried out by the Primary Productivity Algorithm Round Robin program headed by M.-E. Carr and M. Friedrichs [*Carr et al.*, 2006; *Campbell et al.*, 2003].

2.3. Particle Export

[7] The ratio of particulate organic carbon (POC) export to primary production (the pe-ratio) was taken from *Dunne et al.* [2005] as

$$\mathrm{pe-ratio} = -0.0081 \cdot \mathrm{T} + 0.0806 \cdot \ln(\mathrm{Chl}) + 0.426$$
$$0.04 < \mathrm{pe-ratio} < 0.72 \quad (1)$$

where we have taken surface chlorophyll (mg Chl m^{-3}) estimates from the SeaWiFS satellite and surface temperature estimates (°C) from the NCEP reanalysis. The uncertainty of the pe-ratio component is assumed to be 35% (1 s.d.) after *Dunne et al.* [2005].

2.4. Stoichiometry of Particle Export

[8] In order to account for geographical variability of particle export stoichiometry, we use the technique of *Sarmiento et al.* [2002, 2004] in which the net utilization ratio is obtained from the ratio of vertical concentration gradients using a water column nutrient data set compiled from the WOCE, SAVE, TTO and GEOSECS programs [*Sarmiento et al.*, 2002, 2004]. The mean concentration over the top 100 m is used as the surface value, and the mean in the 100 m to 200 m range as the thermocline, or source, value (e.g., Si:N gradient ratio = $[SiO_4^{100-200} - SiO_4^{0-100}]/[NO_3^{100-200} - NO_3^{0-100}]$). The bootstrap method was used to estimate the nonparametric standard deviation of the mean with 10,000 trial data sets from the original data set by random selection with replacement (i.e., repeatedly selecting from the same set of observations). The most likely estimate of the ratio was then taken as the median of all trials with the 95% confidence

Table 1. Net Uptake Ratios of $CaCO_3$ to C_{org} and Silicon to Nitrogen Estimated From the Data Synthesis[a]

Region	Atlantic	Indian	Pacific
	Ca:C$_{org}$		
Subpolar gyre (>45°N)	0.023 ± 0.020 (170)		0.061 ± 0.007 (97)
Subtropical gyre (15°N–45°N)	0.014 ± 0.019 (185)	0.027 ± 0.017 (43)	0.048 ± 0.011 (195)
Equatorial (15°S–15°N)	0.084 ± 0.005 (304)	0.099 ± 0.004 (352)	0.087 ± 0.005 (302)
Subtropical gyre (45°S–15°S)	0.066 ± 0.016 (204)	0.099 ± 0.014 (305)	0.045 ± 0.017 (282)
Southern Ocean (<45°S)		0.018 ± 0.009 (441)	
	Si:N		
Subpolar gyre (>45°N)	0.54 ± 0.02 (747)		1.97 ± 0.05 (343)
Subtropical gyre (15°N–45°N)	0.30 ± 0.02 (882)	1.13 ± 0.07 (85)	0.91 ± 0.04 (789)
Equatorial (15°S–15°N)	0.31 ± 0.01 (903)	0.91 ± 0.02 (645)	0.75 ± 0.02 (983)
Subtropical gyre (45°S–15°S)	0.33 ± 0.01 (1009)	0.40 ± 0.03 (834)	0.37 ± 0.06 (1041)
Southern Ocean (50°S–45°S)	0.91 ± 0.06 (88)	1.30 ± 0.15 (47)	0.40 ± 0.03 (36)
Southern Ocean (55°S–50°S)	3.01 ± 0.11 (143)	3.62 ± 0.16 (171)	1.27 ± 0.10 (154)
Southern Ocean (60°S–55°S)	4.19 ± 0.11 (159)	5.08 ± 0.18 (79)	3.03 ± 0.16 (169)
Southern Ocean (65°S–60°S)	4.94 ± 0.13 (152)	5.23 ± 0.07 (69)	4.40 ± 0.13 (107)
Southern Ocean (70°S–65°S)	5.59 ± 0.19 (83)	4.00 ± 0.30 (87)	3.98 ± 0.10 (186)
Southern Ocean (90°S–70°S)	3.82 ± 0.39 (135)		0.58 ± 0.11 (108)

[a]Uncertainties are given as one standard deviation of the mean. Ocean regions were defined as by *Sarmiento et al.* [2002] with 20°W dividing the Atlantic from Indian, 140°E dividing the Indian from Pacific, and 70°W dividing the Pacific from Atlantic.

limits from the 2.5% and 97.5% tails of the resulting distribution.

[9] Results for the nutrient utilization ratio of silicon to nitrogen taken from the gradient ratio of silicate to nitrate are reproduced from *Sarmiento et al.* [2004, Table 1] outside the Southern Ocean with more finely resolved estimates within the Southern Ocean. Southern Ocean estimates had a strong latitudinal structure, with maxima near 60°S and low values in the Ross Sea. As described by *Sarmiento et al.* [2004], very low values (below 0.5) were observed in the southern subtropical regions of all ocean basins as well as in the tropical Atlantic and northern subtropical Atlantic.

[10] Results for the nutrient utilization ratio of $CaCO_3$ to POC ratio taken from the gradient ratio of potential alkalinity to nitrate (and converted to carbon using a constant C:N value of 117:16 [after *Anderson and Sarmiento*, 1994] are also shown in Table 1. These values also differ from *Sarmiento et al.* [2002] for the Southern Ocean in that we have taken a single value for the entire Southern Ocean (90°S–45°S) to account for the lack of data in the Indian Ocean and similarity between the Atlantic and Pacific oceans. Values of silicon to nitrogen ratios south of 45°S in this report also differ from those by *Sarmiento et al.* [2004] in that they are provided in more highly resolved, 5° meridional bins in order to more accurately describe the high extent of meridional variability in this region. This change has only a modest impact on the global estimates, reducing the global SiO_2 flux out of the euphotic zone by an average of 6%.

2.5. Fate of Particle Export

[11] The estimates of sinking POC export obtained above were propagated to depth with a variety of algorithms. In order to obtain uncertainty estimates on particle flux penetration length scales, we propagated our estimates through the suite of 11 sediment-trap-based algorithms presented by *Lutz et al.* [2002]. For sensitivity experiments, we utilized the "Martin curve" [*Martin et al.*, 1987] as implemented in the OCMIP2 protocol ($F = F_{75} \times (z/75)^{0.9}$) [*Najjar and Orr*, 1998]. To study regional variability in penetration depth scaling, we used the mineral protection algorithm of *Klaas and Archer* [2002] for which we used single penetration length scales of SiO_2, undersaturated $CaCO_3$, and unprotected organic matter of 2000 m, 3500 m, and 188 m, respectively. Undersaturation of calcite was determined from dissolved inorganic carbon and alkalinity distributions from the Global Ocean Data Analysis Project (http://cdiac.ornl.gov/oceans/glodap/Glodap_home.htm). Mass-based mineral protection ratios of POC by $CaCO_3$, SiO_2, and lithogenic material were assumed to be 0.070, 0.026 and 0.065 after *Klaas and Archer* [2002].

[12] An algorithm for burial efficiency relating the seafloor POC flux to sediment POC burial flux was derived from a synthesis of burial efficiency and sediment composition studies. Because much of the available data on burial efficiency has been presented through the relationship between sediment mass accumulation rates and the preservation efficiency of POC, we derived an algorithm based exclusively on POC. This involved developing two separate algorithms: one for percent organic carbon of surface sediments (%OC) as a function of sediment mass accumulation rate (F_{mass_accum}; g cm^{-2} a^{-1}), and another for sediment POC burial flux (F_{POC_accum}; g C cm^{-2} a^{-1}) as a function of bottom POC flux. To derive a relationship between %POC and F_{mass_accum}, we performed a log linear regression of the data compilation by *Hedges and Keil* [1995]:

$$\%POC = F_{POC\_burial}/F_{mass\_accum} \cdot 100 = 12.0 \cdot F_{mass\_accum}^{0.4} \quad (2)$$

Where necessary, constant sediment porosity ($\phi = 0.7$) and density ($\rho = 2.7$) were assumed to convert between sediment accumulation rates in velocity (e.g., cm ka^{-1}) and flux (e.g., g cm^{-2} a^{-1}) units. This algorithm was found to explain 48% of the observed variance (e.g., $r^2 = 0.48$), and have a median deviation of 50% in the relative sense (e.g., abs(model −

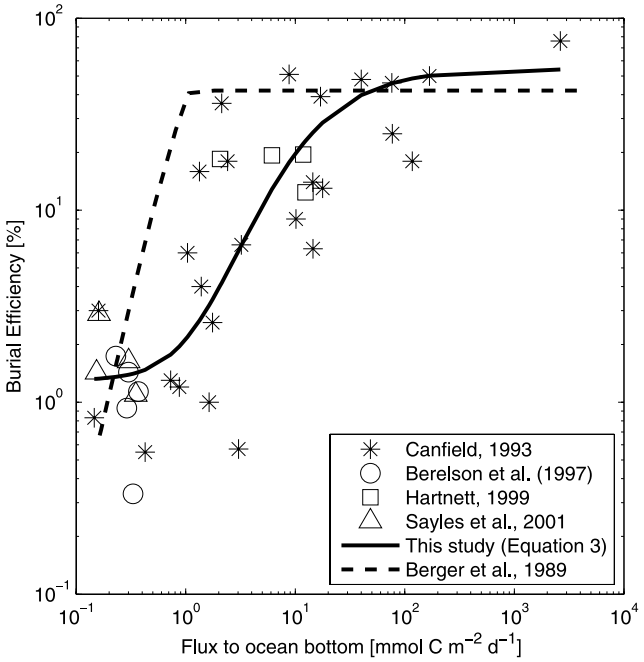

Figure 2. Sediment burial efficiency versus sinking flux to bottom sediments. Data are shown from a global synthesis of oxic sites given by *Canfield* [1993, 1994], Washington state and Mexican continental margins [*Hartnett and Devol*, 2003], equatorial Pacific [*Berelson et al.*, 1997], and the Southern Ocean [*Sayles et al.*, 2001]. Also shown is the data fit from equation (3) as well as the equation given by *Berger* [1989] for which we have used equation (2) to convert between mass and carbon.

data)/data × 100).

[13] We compiled observations of burial efficiency as a function of sediment accumulation rate (*Canfield* [1993, 1994] (oxic sediments only), *Hartnett and Devol* [2003], *Berelson et al.* [1997], and *Sayles et al.* [2001]) and applied equation (2) to convert sediment mass accumulation rate into POC burial flux and generate the following algorithm:

$$F_{POC\_burial} = F_{POC\_bottom} \cdot \left(0.013 + 0.53 \cdot F^2_{POC\_bottom} / (7.0 + F_{POC\_bottom})^2\right) \quad (3)$$

In this case, F_{POC_bottom} is the flux of organic carbon reaching the sediments and F_{POC_burial} is the POC burial flux, both in units of mmol C m^{-2} d^{-1}. Optimal coefficients for this algorithm were found by minimizing logit transformed data-model differences for burial efficiency (Figure 2; logit(x) = ln(x/(1 − x)) where x is the burial efficiency [*Sokal and Rohlf*, 1995]). This algorithm was found to explain 66% of the observed variance with a median deviation of 56% in the relative sense.

[14] The dissolved organic carbon (DOC) flux from sediments was estimated as 14% of the total flux reaching the sediments above 2000 m and 36% below 2000 m after *Papadimitriou et al.* [2002]. While this formulation has the advantage of simplicity, we note that the work of *Burdige et al.* [1999] suggests that it may overestimate DOC flux in shallow, productive sediments.

2.6. Sediment-Based Data Sets Used for Comparison

[15] Sediment mass percentages of biogenic $CaCO_3$, SiO_2, POC, and lithogenic material (by difference) were taken from the global synthesis of *Seiter et al.* [2004] with data maps provided by M. Zabel (personal communication, 2006). Because of the scarcity of point observations and consequent lack of a single, definitive map for sediment accumulation rates, we derived a sediment accumulation map from the geometric mean of two existing maps: that of R. A. Jahnke (personal communication, 1996) and that generated by objectively analyzed extrapolation from available field data compilations provided by D. Archer (personal communication, 2006) and M. Zabel (personal communication, 2006) derived from core top estimates available at the National Oceanic and Atmospheric Administration's National Geophysical Data Center.

2.7. Uncertainty Propagation

[16] We estimated the uncertainty for each data type in the following manner. For the uncertainty in primary production we used the three separate algorithms. For pe-ratio, we used the 35% uncertainty estimate from *Dunne et al.* [2005]. For the stoichiometry estimates, we used the uncertainty in the mean gradient ratios given in Table 1. For the attenuation of organic carbon through the water column, we propagated our estimates through the suite of 11 sediment-trap-based algorithms presented by *Lutz et al.* [2002]. For the burial efficiency, we used the 50% uncertainty estimate from the regression derived in equation (3) from Figure 2. The overall uncertainty was then estimated as the standard deviation of all 33 combinations of aerially and temporally varying flux estimates (3 primary production × 11 flux attenuation).

3. Results

3.1. Particle Export

[17] Zonal integrals of primary production (Figure 3a) and particle export (Figure 3b) from the three primary production algorithms all show prominent maxima in the equatorial and southern subpolar regions, with a weaker maximum in the northern subpolar region. The satellite-based estimates of particle export have a smaller range than the satellite-based primary production estimates with an 8% smaller standard deviation in the zonal means and 30% smaller standard deviation in the global integral. This reduction is due to the opposing effects of temperature in the primary production algorithm, where it is generally positive, and the pe-ratio algorithm, where it is negative. By contrast, the conversion from primary production to particle export approximately doubles the flux difference between the (low-chlorophyll) subtropics and the (higher-chlorophyll) equatorial and subpolar regions since chlorophyll is positively correlated with both primary production and pe-ratio. Because of this, while the initial primary

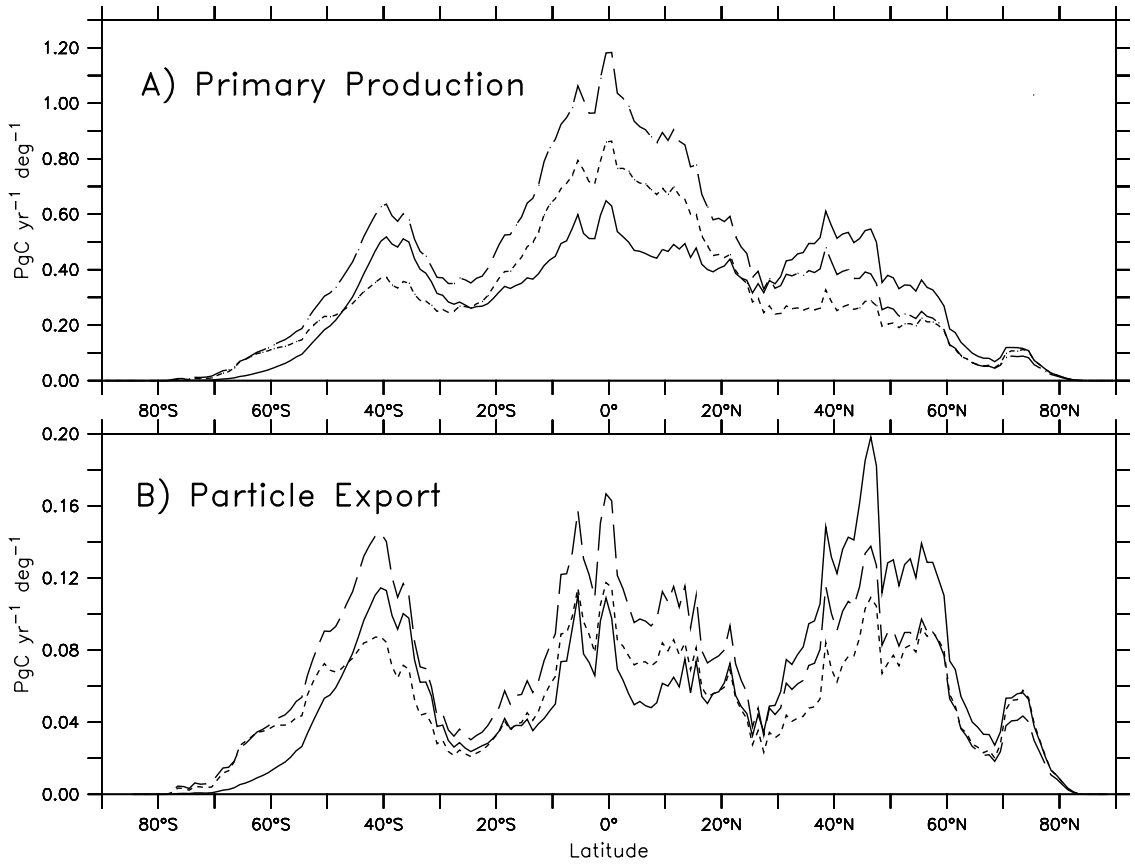

Figure 3. Zonal integrals of primary production (a) and particle export (b) in units of Pg C a^{-1} deg^{-1}. Lines represent the three primary productivity algorithms of *Behrenfeld and Falkowski* [1997] (solid line), *Carr* [2002] (dashed line), and *Marra et al.* [2003] (dotted line).

production estimates exhibit a pronounced equatorial maximum, the average particle export and variability between algorithms is lowered in the equatorial region relative to the subpolar regions such that they each become similar in magnitude and the subtropical minima become more pronounced.

[18] A note about the regridding onto the Levitus mask is warranted. In contrast to the standard SeaWiFS mask, the Levitus mask predominantly counts cells with fractional land (such as coastlines and islands) as being completely land. While this discrepancy affects only 2.9% of the ocean area, that area corresponds to 16% of the SeaWiFS-based primary production. Because these areas are both highly productive and shallow, the algorithms developed here infer them to be extremely efficient at exporting and burying particles. Decisions about how these regions are treated thus have a large impact on our estimates of coastal production and global burial, and deserve more comprehensive and thorough study.

[19] Temporal variability in forcing fields and the resulting particle export is shown in Figure 4, in terms of the Northern Hemisphere integral, Southern Hemisphere integral, and global integral. Because of the larger ocean area in the Southern Hemisphere (2.03×10^{14} m^2) than in the Northern Hemisphere (1.47×10^{14} m^2), the maximum irradiance reaching the surface ocean is in December and the minimum in June (black line in Figure 4a). Global average sea surface temperature varies only slightly (black line in Figure 4b) as the relatively larger excursion in the Northern Hemisphere is balanced by the larger area of the Southern Hemisphere. Global chlorophyll, on the other hand, demonstrates marked variability as it correlates with the Northern Hemisphere variability. In our analysis, the strong chlorophyll forcing outweighs the irradiance forcing such that particle export has a much higher summer seasonal peak in the Northern Hemisphere ($\sim$7.6 Pg C a^{-1}) than in the Southern Hemisphere ($\sim$5.5 Pg C a^{-1}). Overall, particle export averaged 9.6 Pg C a^{-1} and varied seasonally with a minimum in March (average 8.9 Pg C a^{-1}) and a maximum in August (average 11.2 Pg C a^{-1}) with 88% of the temporal variance being intra-annual. Our estimate of global particle export, driven by area-weighted seasonal variability in chlorophyll, temperature and irradiance, is thus anticorrelated with the globally integrated ocean surface irradiance as this driver is outweighed by the high particle export in the subpolar and polar North Atlantic and (less so) North Pacific.

[20] Regional and global export estimates for organic carbon, $CaCO_3$, and SiO_2 in sinking particles derived from the algorithm are given in Table 2. Areally integrated POC

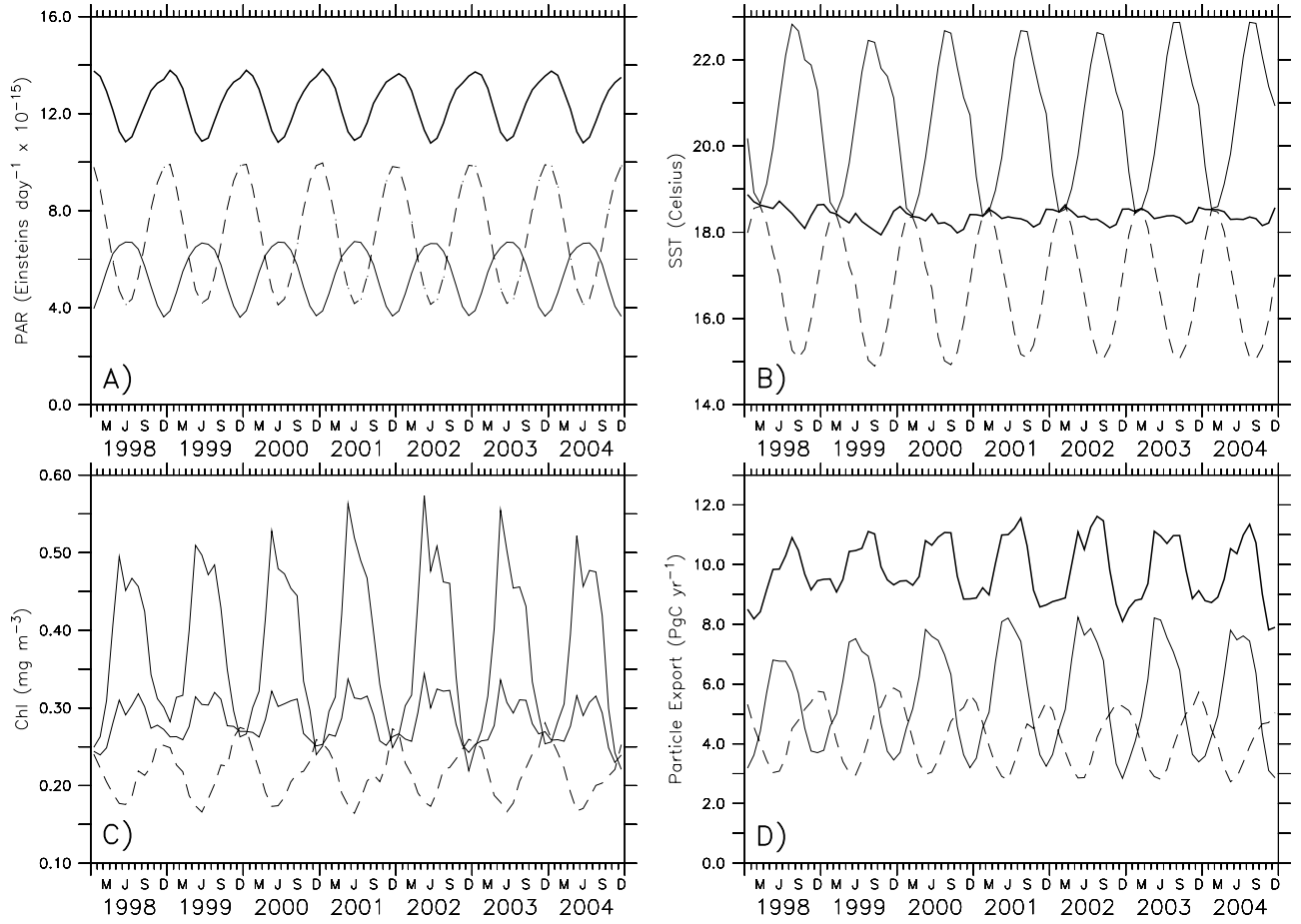

Figure 4. Monthly variability of average PAR (Einstein's $d^{-1} \times 10^{-15}$), SST (°C), and chlorophyll (mg m^{-3}), the forcing parameters for the particle export within our model, and integrated particle export (Pg C a^{-1}). Results are broken down into global (black line), northern (gray line), and southern (dashed line) domains.

export is relatively equally weighted by ocean region with the exception of high export in the equatorial Pacific and low export in the Southern and subtropical Indian oceans. $CaCO_3$ export has maxima in the equatorial regions while SiO_2 has maxima in the subpolar and polar regions. SiO_2 export has large contrasts between regions, with very low values in the southern subtropical gyres.

[21] The time series of hemispheric POC export (Figures 3 and 4) and regionally integrated POC export (Table 2) demonstrate the strong asymmetry between the hemispheres outside the equatorial zone. While the ocean area poleward of 15 degrees is twice as large in the Southern Hemisphere as in the Northern Hemisphere, the POC export and SiO_2 are both significantly greater in the Northern Hemisphere. This asymmetry can be traced back to the relatively low chlorophyll in the subpolar Southern Ocean and high chlorophyll in the North Atlantic. While one possible cause of this asymmetry may be the much higher windborne flux of iron to the Northern Hemisphere [e.g., *Gao et al.*, 2003], other causes such as light limitation in deep summertime Southern Ocean mixed layers, or even systematic underestimation of the chlorophyll content and primary productivity in such deep mixed layers cannot be ruled out at present.

3.2. Penetration of Export Flux to Deep Sea Sediments

[22] In this section, we compare our satellite-based fluxes of organic carbon to the seafloor with those based on the synthesis of deep-sea sediment observations. For the sediment-based estimate (Figure 5a), the total POC flux to the seafloor is assumed to be the sum of remineralized organic carbon flux from benthic oxygen flux maps given by *Jahnke* [1996] and the organic carbon burial flux from the sediment accumulation rates derived above multiplied by the organic carbon contents from *Seiter et al.* [2004]. This comparison allows us to not only independently evaluate the fidelity of the satellite-based export approach but, insofar as the satellite-based POC export sediment-based bottom POC flux approaches are valid, to consider the factors governing the penetration of POC through the water column in greater detail.

[23] We assess the bias of five different methods for depth attenuation of satellite-derived organic carbon flux (Figures 3–4) relative to the sediment-based estimate in

Table 2. Particle Export of Organic Carbon, $CaCO_3$, and SiO_2 From the Combined Satellite Primary Production and Particle Export Algorithms and Net Utilization Ratios[a]

Region	Atlantic	Indian	Pacific
Area ($\times 10^{13}$ m^2; 34.84 Total)			
Arctic (Atl > 80°N, Pac > 65°N)		1.06	
Subpolar gyre (>45°N)	0.89		0.96
Subtropical gyre (15°N–45°N)	2.46	0.28	3.91
Equatorial (15°S–15°N)	1.99	2.48	5.72
Subtropical gyre (45°S–15°S)	2.11	2.93	4.31
Southern Ocean (<45°S)	1.49	1.71	2.54
Total	8.94	7.40	17.44
Organic C (Pg C a^{-1}; 9.6 Total)			
Arctic (Atl > 80°N, Pac > 65°N)		0.51	
Subpolar gyre (>45°N)	0.77		0.77
Subtropical gyre (15°N–45°N)	0.75	0.32	0.97
Equatorial (15°S–15°N)	0.83	0.65	1.09
Subtropical gyre (45°S–15°S)	0.75	0.57	0.61
Southern Ocean (<45°S)	0.35	0.27	0.38
Total	3.45	1.81	3.82
$CaCO_3$ (Pg C a^{-1}; 0.52 Total)			
Arctic (Atl > 80°N, Pac > 65°N)		0.012	
Subpolar gyre (>45°N)	0.018		0.047
Subtropical gyre (15°N–45°N)	0.010	0.009	0.046
Equatorial (15°S–15°N)	0.067	0.065	0.095
Subtropical gyre (45°S–15°S)	0.049	0.057	0.027
Southern Ocean (<45°S)	0.006	0.005	0.007
Total	0.150	0.136	0.222
Si (Tmol a^{-1}; 99 Total)			
Arctic (Atl > 80°N, Pac > 65°N)		3.2	
Subpolar gyre (>45°N)	4.8		17.3
Subtropical gyre (15°N–45°N)	2.5	4.1	12.4
Equatorial (15°S–15°N)	3.0	6.7	9.3
Subtropical gyre (45°S–15°S)	2.8	2.6	2.5
Southern Ocean (<45°S)	10.4	9.902	7.7
Total	23.5	23.3	49.2

[a]We assume a carbon to nitrogen ratio of 117/16 after *Anderson and Sarmiento* [1994].

terms of the log of the ratio of the satellite to sediment-based estimates (Figure 5a) for water depths greater than 1000 m between 60°N and 60°S in Figure 5. Results using the classic *Martin et al.* [1987] (henceforth Martin) curve are shown in Figure 5b. Globally integrated, this attenuation factor leads to an organic carbon flux to sediments of 0.146 Pg C a^{-1}, only 8% higher than the sediment-based flux estimate of 0.131 Pg C a^{-1}. Regionally, however, the flux to the sediment based on the Martin curve underestimates the flux in the off-equatorial tropics and subtropics and overestimates the flux in subpolar regions relative to the sediment-based estimate. The Martin-based sediment flux explains only 15% of the geographical variance with a standard deviation of 0.40 log10 units.

[24] The regional biases in this comparison suggests that either the satellite-based estimate of particle export has both a low bias in the tropics and a high bias in the subpolar regions, or that particles penetrate deeper than the Martin curve in the tropics and shallower than the Martin curve in subpolar regions. As we demonstrate in the following discussion, the latter explanation is consistent with current understanding of controls on POC penetration by mineral protection. The level of regional fit improved considerably when the regionally varying penetration scheme of mineral protection algorithm from *Klaas and Archer* [2002] was used, but only when the role of lithogenic material (clay) was included in the penetration.

[25] In order to explore the sensitivity of bottom POC flux to the implementation choice of the *Klaas and Archer* [2002] algorithm, we present the sequential addition of terms in Figures 5c–5f. Using only protection by SiO_2 and $CaCO_3$ (Figure 5c), underestimates the globally (60°N–60°S) integrated bottom flux (0.103 Pg C a^{-1}) relative to the sediment-based estimate by 24% with only 21% of the geographical variance being explained and a standard deviation of 0.49 log10 units. The most prominent biases in Figure 5c are the large area in the North Atlantic that is underestimated by an order of magnitude and the broad areas in the North and South Pacific underestimated by factors of 2–8. The fact that our global estimate of $CaCO_3$ export (0.52 ± 0.15 Pg C a^{-1}) is considerably lower than many of the previous estimates (Table 3) prompted us to explore the sensitivity of our result to our choice of input data with two tests: (1) doubling the value of $CaCO_3$ export used in the penetration algorithm (Figure 5d) and (2) using the maximum of the original $CaCO_3$ export estimate and $CaCO_3$ from sediment accumulation rates directly (not shown). Doubling the $CaCO_3$ export overestimates the flux relative to that derived from sediment data by 45% and correlating with slightly less geographical variance (20%) than the previous test. One improvement was in decreasing the relative standard deviation to 0.42 log10 units. Including the sediment $CaCO_3$ data in the penetration estimate (not shown) provided a moderate improvement in the fit in a few areas, but did not ameliorate the large-scale biases. From these $CaCO_3$ sensitivity studies, we conclude that the bulk of the low bias in Figure 5b cannot be explained as due to underestimation of the role of $CaCO_3$ in transfer of organic carbon to the seafloor.

[26] While the original analysis of Klaas and Archer suggested that lithogenic material played a minor role, the lack of consistency between the satellite and sediment-based estimates using the methods described above (Figure 5b) led us to test an alternate hypothesis: that lithogenic material plays a large role in protection of organic matter, particularly in areas of low surface flux. Including an estimate of lithogenic mineral supply of 0.43 Pg a^{-1} based on atmospheric dust deposition [*Ginoux et al.*, 2001] (Figure 5e) provided a moderate but significant improvement to the comparison with sediment data over that with biogenic mineral alone (Figure 5b). The global integral increases to 0.123 Pg C a^{-1} with 23% of the geographical variance explained and a standard deviation of 0.36 log10 units. Much of the low bias in the North Atlantic is removed, and the Pacific bias is partially ameliorated. In this case, lithogenic material accounts for 16% of the bottom POC flux (depths greater than 1000 m). This result is significantly higher than the 5–6% estimated by *Klaas and Archer* [2002]. However, when the much greater lithogenic flux of 1.37 Pg a^{-1} inferred from our sediment observation synthesis is included in the protection scheme, the amount of lithogenic flux is increased dramatically and a globally robust comparison is achieved (Figure 5f). Including these

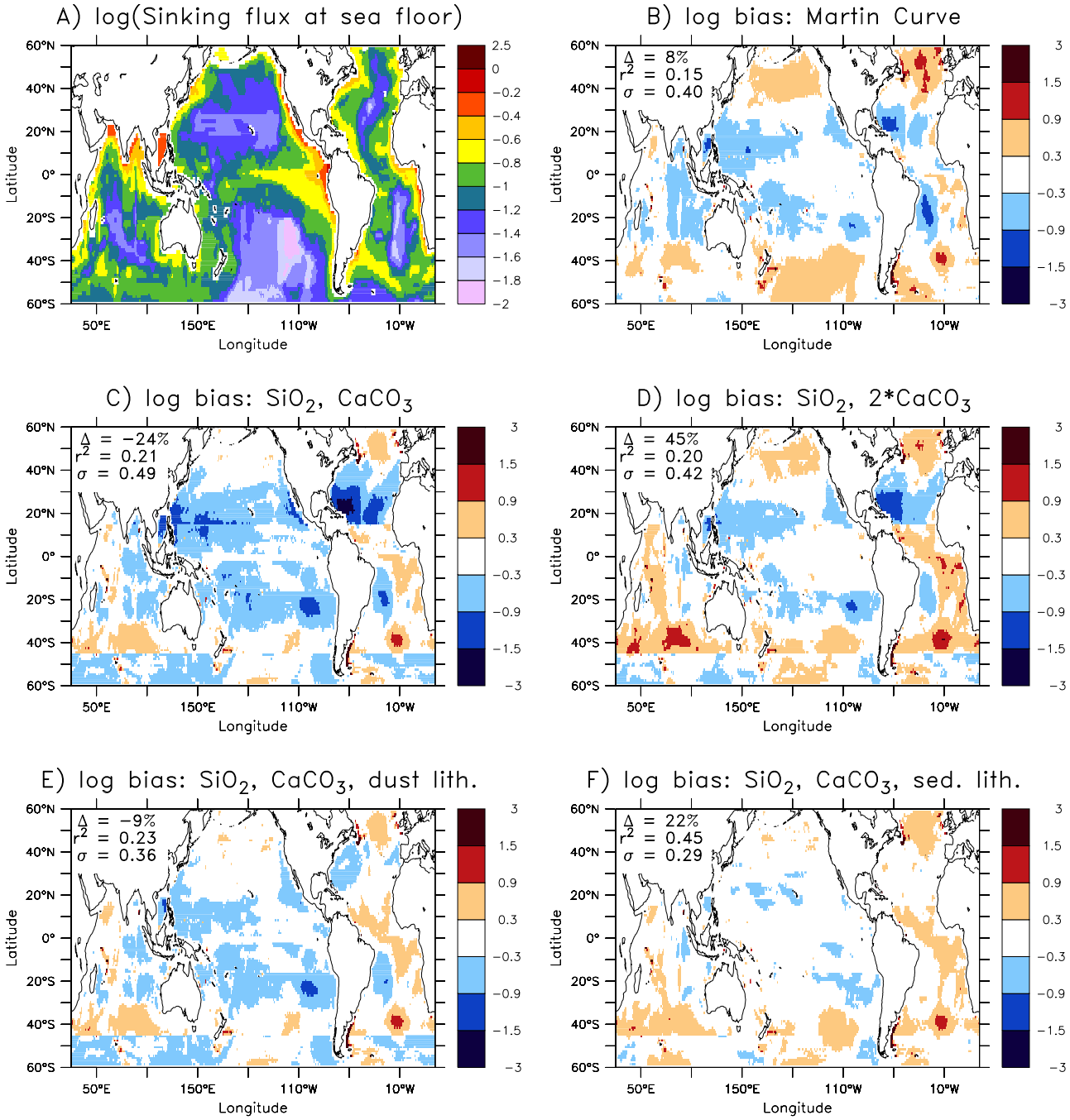

Figure 5. The log10 of the particulate organic carbon flux (mmol m^{-2} d^{-1}) to the seafloor based on sediment derived estimates of benthic oxygen consumption rates from *Jahnke* [1996] converted to organic carbon using a factor of 0.6 plus the sediment POC accumulation rates described in the text (a) used for comparison with satellite-derived estimates in Figures 5b–5f. In each case, the value shown is the log10 ratio of seafloor organic carbon fluxes derived from SeaWiFS satellite over those derived from sediment data syntheses contrasting algorithms for the penetration of POC from the surface to the seafloor (water depths >1000 m; 60°S to 60°N). In all cases, the denominator is the sediment-derived value in Figure 5a. Flux penetration was given by the *Martin et al.* [1987] curve in Figure 5b and variants of the *Klaas and Archer* [2002] parameterization in all the others: (c) Only SiO_2 and $CaCO_3$; (d) as in Figure 5c except with doubling the $CaCO_3$; (e) as in Figure 5c except including lithogenic flux from aeolian dust input of *Ginoux et al.* [2001]; (f) as in Figure 5c except including lithogenic flux derived from the accumulation of lithogenic material in sediments.

Table 3. Comparison of Our POC Export Fluxes With Other Estimates[a]

	This Study	Previous Studies
	POC (Gt a^{-1})	
Global export	9.6 ± 3.6	11.1–12.9 [*Laws et al.*, 2000][b]
		9.2 [*Aumont et al.*, 2003][c]
		8.6 [*Heinze et al.*, 2003][c]
		8.7–10.0 [*Gnanadesikan et al.*, 2004][c]
		9.6 [*Schlitzer*, 2004][d]
		5.8–6.6 [*Moore et al.*, 2004][c]
Export flux south of 50°S	0.69 ± 0.26	1.1 ± 0.2 [*Pollard et al.*, 2006][b]
Global flux to bottom	2.3 ± 0.9	0.93 [*Muller-Karger et al.*, 2004][b]
Burial in margins (50–2000 m)	0.29 ± 0.15	0.06 [*Muller-Karger et al.*, 2004][b]
Burial in deep sea (>2000 m)	0.012 ± 0.02	0.09 [*Muller-Karger et al.*, 2004][b]
Flux across 1000 m 60°S–60°N	0.63 ± 0.22	0.86 [*Jahnke*, 1996][b]
		0.71–0.86 [*Gnanadesikan et al.*, 2004][c]
Flux across 2000 m 30°S–47°N	0.20 ± 0.08	0.16 ± 0.11 [*Ganachaud and Wunsch*, 2002][d]
		0.22–0.32 [*Gnanadesikan et al.*, 2004][c]
	$CaCO_3$ (GtC a^{-1})	
Global export	0.52 ± 0.15	0.9–1.1 [*Lee*, 2001][b]
		1.8 [*Heinze et al.*, 1999][c]
		1.64 [*Heinze et al.*, 2003][c]
		0.68–0.78 [*Gnanadesikan et al.*, 2004][c]
		0.38 [*Moore et al.*, 2004][c]
		0.84 [*Jin et al.*, 2006][c]
		0.5–4.7 [*Berelson et al.*, 2007][b]
Export to 2000 m	0.29 ± 0.15	0.6 ± 0.4 [*Berelson et al.*, 2007][b]
Export, Atlantic	0.16	0.13 [*Chung et al.*, 2003][b]
Export, Pacific (>40°S)	0.21	0.31 [*Feely et al.*, 2002][b]
Export, Indian	0.12	~0.1 [*Sabine et al.*, 2002][b]
	Silicon (Tmol a^{-1})	
Global export	101 ± 35	100–140 [*Nelson et al.*, 1995][b]
		70–100 [*Gnanadesikan*, 1999][b]
		80–90 [*Gnanadesikan*, 1999][c]
		170 [*Heinze et al.*, 1999][c]
		148–185 [*Heinze et al.*, 2003][c]
		106 [*Aumont et al.*, 2003][c]
		69 [*Moore et al.*, 2004][c]
		180 [*Jin et al.*, 2006][c]
Global flux to bottom	22.1	40 [*Nelson et al.*, 1995][b]
		29 [*Treguer et al.*, 1995][b]
		58 [*Heinze et al.*, 2003][c]
Flux across 2000 m 30°S–47°N	11.2	12.3 ± 7.5 *Ganachaud and Wunsch* [2002][b]
Export flux south of 30°S	33 ± 4	17–37 [*Nelson et al.*, 1995][b]
		23–38 [*Gnanadesikan*, 1999]
		50–80 [*Pondaven et al.*, 2000][b]/[*Nelson et al.*, 2002][b]
Export flux south of 50°S	25 ± 4	51 ± 3 [*Pollard et al.*, 2006][b]
Export flux in eastern	4.9 ± 1.1 (10°N–10°S)	~10 [*Dunne et al.*, 1999][b]
equatorial Pacific	2.0 (5°N–5°S)	10–14 [*Gnanadesikan*, 1999][c]
		2.0 [*Jiang et al.*, 2003][c]

[a]Model range from *Gnanadesikan et al.* [2004] are the two "best-guess" models with the best match to phosphate, AOU, and radiocarbon.
[b]Data-based estimates.
[c]Estimates using numerical general circulation models.
[d]Estimates based on inversion (geostrophic or adjoint).

presumably riverine and directly erosional sources of lithogenic material increases the global integral rises to 0.165 Pg C a^{-1} and the explained geographical variance rises to 45%: a threefold increase in correlation over that from the Martin curve. Similarly, the standard deviation is reduced to 0.29 log10 units, equivalent to a better than twofold improvement of local agreement between these estimates. Disagreements exist, however, with the mid-Atlantic ridge now being represented as a regional overestimate. Additional sensitivity experiments demonstrated that the agreement could be improved considerably through utilization of a simpler $CaCO_3$ dissolution scheme of a single penetration length scale of 3500 m used in OCMIP-II [*Najjar and Orr*, 1998] (not shown). While this sensitivity test gave unrealistically low fluxes of $CaCO_3$ to the seafloor, it improved the comparison with sediment-based organic carbon fluxes considerably by ameliorating the high bias in the mid-Atlantic ridge. In this case, lithogenic material served as the dominant protective phase for organic material transport to the deep seafloor, accounting for 51% of the total POC flux.

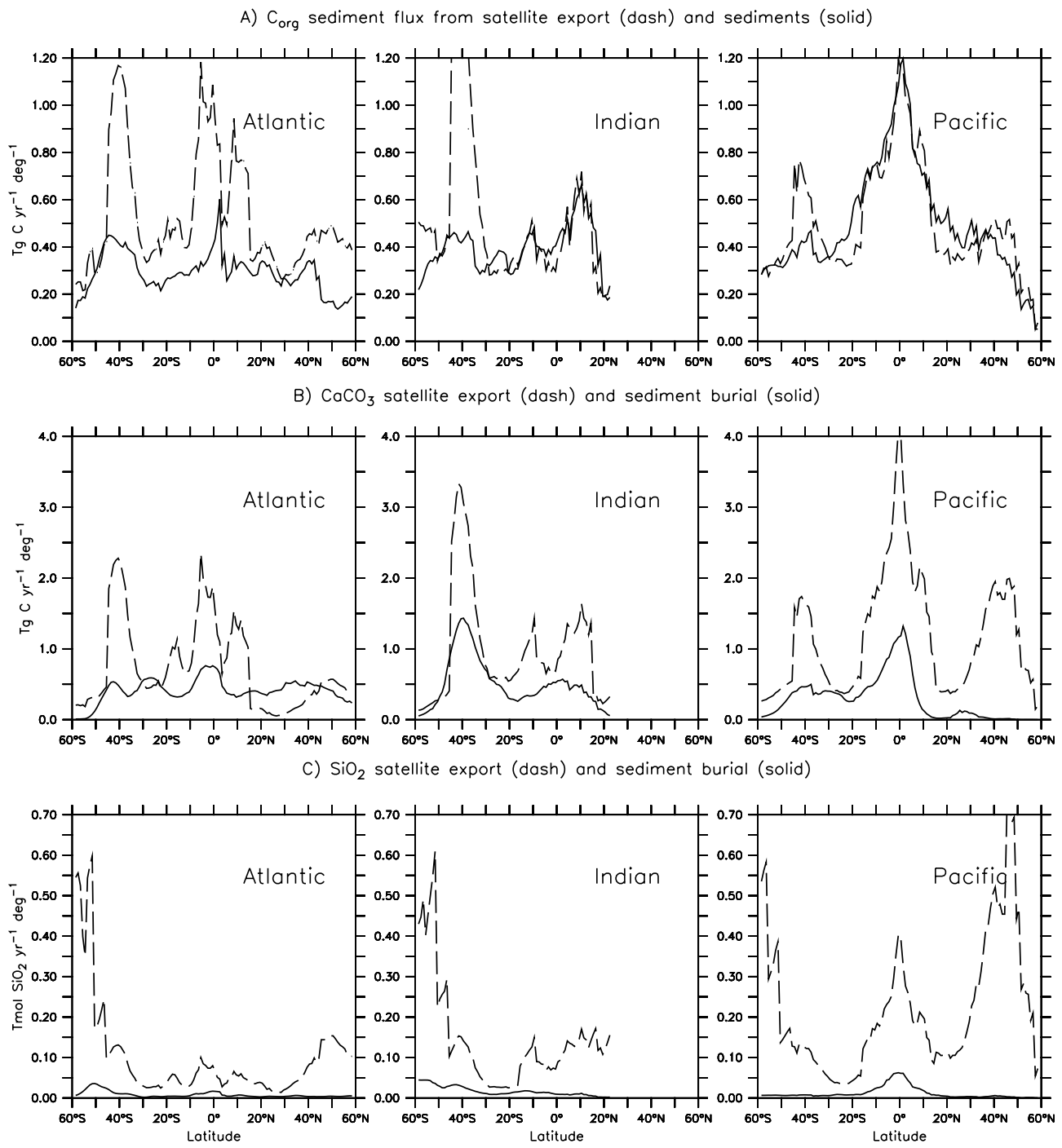

Figure 6. (a) Zonally integrated organic carbon flux at the seafloor (water depths greater than 1000 m) from the satellite-derived estimate corresponding to that in Figure 4f (dashed line), and the sediment-derived estimate (solid line). (b) Zonally integrated satellite-derived $CaCO_3$ export fluxes (dashed line) and sediment-derived accumulation fluxes (solid line). (c) Zonally integrated satellite-derived SiO_2 export fluxes (dashed line) and sediment-derived accumulation fluxes (solid line).

[27] Ocean basin zonal integrals (water depths greater than 1000 m, 60°N–60°S) in Figure 6a compare the sediment-based seafloor POC flux estimate with the satellite-based estimate in Figure 5f. With the exception of the high satellite-based values near 40°S in the Atlantic and Indian oceans, these two independent estimates of the organic carbon flux to the seafloor show remarkable similarity in both overall magnitude and latitudinal structure.

[28] As another check on the internal consistency of this analysis, we compare ocean basin zonal integrals (water depths greater than 1000 m, 60°N–60°S) for satellite-based export and sediment-based burial estimates of $CaCO_3$

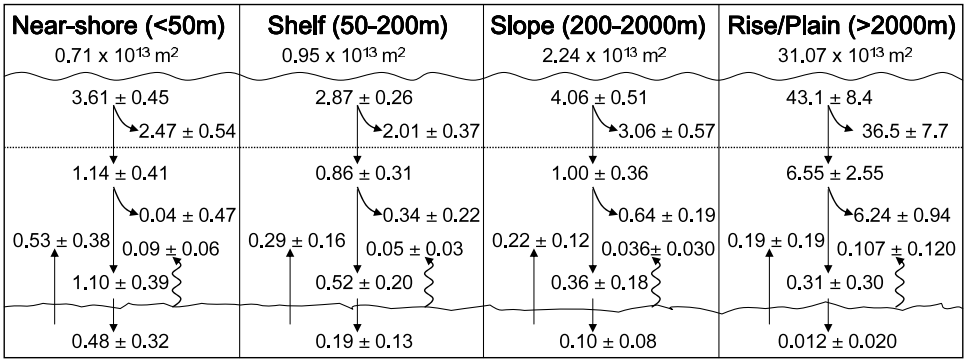

Figure 7. Synthesis of organic carbon fluxes broken down by depth regimes. Down arrows are organic carbon fluxes (Pg a^{-1}). Curved arrows and straight up arrows are remineralization fluxes. Squiggly up arrows are dissolved organic carbon fluxes.

(Figure 6b) and SiO_2 (Figure 6c). General consistency is demonstrated in our estimates of satellite-based $CaCO_3$ export being greater or equal to sediment-based burial with an implied average preservation of $CaCO_3$ through the water column and in surface sediments of 40%. However, the two estimates demonstrate some inconsistency in the subtropical North Atlantic wherein sediment-based burial exceeds satellite-based supply. We suspect this discrepancy is due to a low bias in our estimates of the $CaCO_3$ to POC ratio for this region due to the large freshwater and associated alkalinity supply from rivers emptying into the North Atlantic surface waters leading to a breakdown of the simple vertical supply model and an underestimate of the in situ alkalinity utilization. Satellite-based SiO_2 export is everywhere greater than sediment-based burial with an implied average preservation of SiO_2 through the water column and into surface sediments of 7.6%. Our results are thus consistent with those of *DeMaster* [2002] who implicated a high degree of recycling of silicon in the water column and sediments and a large role for shelf and slope regions in global burial.

[29] We consider the good agreement between these estimates both encouraging support of the theory of mineral protection as put forth by *Klaas and Archer* [2002] and other papers [*Armstrong et al.*, 2002; *Francois et al.*, 2002] and indication of a heretofore unappreciated role of lithogenic mineral as a carrier phase for organic material to the deep sea. Surprisingly, lithogenic material proves to be the second most important carrier phase of mineral material in our analysis, 16–51% of the POC flux depending on the magnitude of lithogenic carrier phase. $CaCO_3$ remains the dominant carrier phase with 56% (sensitivity range of 42–76%) with SiO_2 accounting for 6% and unprotected organic material a meager 0.05%. Interestingly, the global flux of atmospheric dust from *Ginoux et al.* [2001] only accounts for 31% of the sediment-based lithogenic flux. This disparity suggests that a majority of this material may be riverine or directly erosional in origin.

3.3. Overall Fate of Primary Production

[30] A summary of the global fluxes of organic carbon inferred from the suite of algorithms is provided in Figure 7 including error estimates. In describing the fate of primary production, we found it convenient to divide the globe in terms of hypsometry, rather than by ocean region, so as to emphasize the dominance of the shelves in the burial of organic material. Whereas the continental shelves, as defined by the 200 m depth horizon, comprise only 5% of the global ocean area in the Levitus mask, we find their significance increases drastically when biogeochemical processes are considered, consistent with previous work [e.g., *Muller-Karger et al.*, 2004]. We estimate that 12% of the primary production (6.5 ± 0.7 Pg C a^{-1}), 21% of the particle export (2.0 ± 0.7 Pg C a^{-1}), 71% of the flux to sediments (1.6 ± 0.6 Pg C a^{-1} total), 85% of the total burial flux (0.67 ± 0.45 Pg C a^{-1}), and 48% of dissolved organic matter release (0.13 ± 0.09 Pg C a^{-1}) occur on the shelves.

[31] Continental slope regions of 200–2000 m are also disproportionately important to the global carbon cycle relative to deeper waters. While the slope accounts for only 7% of the open ocean area, it accounts for a slight majority of the open ocean particulate organic carbon flux to sediments (53%) and a vast majority of open ocean organic carbon burial (89%). This leaves the majority of ocean area (89%) as dominating global primary production (80%) and particle export out of the surface (69%), but corresponding to tight interior recycling such that this large region provides only 2% of global sediment burial in our budget estimate.

[32] Our results differ significantly from recently published work by *Muller-Karger et al.* [2004], who also used SeaWiFS satellite chlorophyll but estimated a much lower global burial (0.22 Pg C a^{-1}) than this study (0.79 Pg C a^{-1}). The greatest source of the difference arises from our inclusion of the nearshore (0–50 m water depths) which accounts for a full 0.48 Pg C a^{-1} of this difference. However, we also predict more burial of organic carbon in the shelf and slope regions and less burial in the deep sea than Muller-Karger et al. This difference stems from a number of sources. First, our global primary productivity (average of *Behrenfeld and Falkowski* [1997], *Carr* [2002], and *Marra et al.* [2003], algorithm) is 12% higher than Muller-Karger et al.'s, but our estimate of the fraction occurring within the 50–2000 m continental margin is 23% lower. This counteracts the effect of their having used

a constant ratio of particle export to net primary production (0.2 across 50 m) while ours varies with temperature and chlorophyll concentration (equation (1)), favoring particle export on highly productive shelves. Finally, our burial efficiency is simply a function of bottom POC flux (Figure 2) and is both much higher than their globally averaged value of 10% on the shelf and much lower than this in the deep sea.

4. Discussion

4.1. Particle Export

[33] Given that the export flux of biogenic matter out of the euphotic zone is one of the primary drivers of ocean biogeochemical cycling, it is important to determine its magnitude. A synthesis of these fluxes is presented in terms of ocean regions in Table 2 and compared with previous estimates in Table 3. Our central estimate of POC export of 9.6 ± 3.6 Pg C a^{-1} is slightly lower than the satellite-based *Laws et al.* [2000] estimate of 11.1 Pg C a^{-1}. However, the *Laws et al.* [2000] estimate includes export through transport of dissolved organic carbon (DOC) in addition to particle sinking, which ours does not. *Hansell and Carlson* [1998] estimate that about 20% of the net community production occurs in the form of DOC, which would increase our value for new production to 12.3 ± 4.0. As seen in Table 3, our central estimate of POC flux is extremely close to the estimates of a number of circulation models [*Aumont et al.*, 2003; *Heinze et al.*, 2003; *Gnanadesikan et al.*, 2004] and to the value of the inverse model of *Schlitzer* [2004]. The recently published model of *Moore et al.* [2004] is somewhat lower than these estimates.

[34] *Gnanadesikan et al.* [2002] noted that diagnostic models which restore surface nutrients toward observations produce rates of biological cycling that depend strongly on the vertical diffusion coefficient and suggested that satellite-based observations might be used to put constraints on the rate of vertical exchange. *Gnanadesikan et al.* [2004] found that the particle export in a suite of such models varied between a low value of 6.9 GtC a^{-1} (low vertical diffusion and weak vertical exchange in the Southern Ocean) to a high value of 13.1 GtC a^{-1} (high vertical diffusion). While this study is unfortunately not sufficiently precise to constrain mixing within forward models, it does suggest an increasing broad consensus between approaches of global POC export being 10 ± 3 Pg C a^{-1}.

[35] This degree of consensus is not yet available for mineral $CaCO_3$ and has been recently described in detail by *Berelson et al.* [2007]. Our estimate of the export of $CaCO_3$ of 0.52 ± 0.15 Pg C a^{-1} is significantly less than the *Milliman and Troy* [1999] estimate of 0.70 Pg C a^{-1}, and much less than the *Lee* [2001] estimates of 0.9–1.1 Pg C a^{-1}. *Berelson et al.* [2007] give a range of estimates of 0.5–1.6 Pg C a^{-1} based on a satellite-based estimate of plankton calcification rates, 1.4–4.7 Pg C a^{-1} based on surface sediment traps, and 1.6 Pg C a^{-1} based on the combination of an estimate of upper water column dissolution of 1.0 Pg C a^{-1} and an estimate of the export to sediment traps at 2000 m of 0.6 ± 0.4 Pg C a^{-1}. Model results range from 0.38 to 1.64 Pg C a^{-1} [*Heinze et al.*, 1999, 2003; *Gnanadesikan et al.*, 2004; *Moore et al.*, 2004; *Jin et al.*, 2006] (Table 3). This discrepancy is particularly important in the Southern Ocean, where a number of models using the OCMIP-like protocols suggested a rain ratio near 0.08 [e.g., *Jin et al.*, 2006], while the work of *Feely et al.* [2002] and *Sarmiento et al.* [2002] suggest a much lower value. If one removes $CaCO_3$ fluxes south of 50°S within the models of *Gnanadesikan et al.* [2004], the resulting global export flux ranges between 0.46 and 0.66, essentially overlapping our estimate. As discussed above for the North Atlantic, we suspect that the large alkalinity supply to surface waters may lead to significant underestimation of the $CaCO_3$ to POC ratio by the *Sarmiento et al.* [2002] method in that region. Alternatively, *Jin et al.* [2006] have also argued that this method underestimates the net $CaCO_3$ to organic carbon ratio by up to 50% because of the vertical gradient method neglecting horizontal transport processes, specifically DOC transport, and because their mean ratios were computed by area-weighted averaging rather than flux-weighted averaging, of particular importance in the Southern Ocean.

[36] Much of the analysis hinges on assumptions regarding the dissolution depth scale of $CaCO_3$. *Chung et al.* [2003] and *Feely et al.* [2002] have suggested that much of the excess alkalinity in the upper waters could be due to the dissolution of particles within the upper water column. *Friis et al.* [2006] suggested that the excess alkalinity in the upper water column could be derived from dissolution of CaCO3 from the sediment. The role of river-derived alkalinity on these estimates is also uncertain, but potentially important [e.g., *Lee et al.*, 2006].

[37] Quantification of global SiO_2 export has also been somewhat controversial. As shown in Table 3, literature values of SiO_2 export flux range between 70 and 185 Tmol Si a^{-1} Our estimate of SiO_2 export of 100.1 ± 35.5 Tmol Si a^{-1} is similar to the lower databased values [*Treguer et al.*, 1995; *Nelson et al.*, 1995; *Gnanadesikan*, 1999] which range between 70 and 140 Tmol Si a^{-1}. It is also consistent with the model-based values proposed by *Gnanadesikan* [1999] for models which include the *Gent and McWilliams* [1990] eddy parameterization and have low vertical diffusivity.

[38] One major source of disagreement in the models is the SiO_2 export in the Southern Ocean. Models differ greatly in how much convection they predict in the Southern Ocean, with simulations which do not have the *Gent and McWilliams* [1990] parameterization giving a lot of convection and high inferred Southern Ocean SiO_2 export (69–171 Tmol Si a^{-1} [*Gnanadesikan*, 1999]) and simulations which include it giving low values (23–38 Tmol Si a^{-1} [*Gnanadesikan*, 1999]). Coarse resolution models in which convection is the dominant mechanism by which radiocarbon is delivered to the deep Southern Ocean have SiO_2 export values that are much higher than the 33 Tmol Si a^{-1} we obtain (Table 3). Our estimates agree with those of *Nelson et al.* [1995] but conflict with higher in situ estimates by *Pondaven et al.* [2000] and *Nelson et al.* [2002] of 50–80 Tmol a^{-1}. Because all in situ measurements (whether sediment traps, bottom SiO_2 flux, or SiO_2 incorporation) require broad geographical extrapolation

over a highly heterogeneous environment, it is difficult to determine the relative robustness of these estimates.

[39] Another area where models often disagree both with each other and with observations is the equatorial Pacific. Modeling studies [e.g., *Gnanadesikan and Toggweiler*, 1999; *Gnanadesikan et al.*, 2002, 2004] have shown the character of this upwelling to be very sensitive to the details of vertical diffusion, and that high vertical diffusion coefficients generally lead to excessive production. Our estimate of 4.5 Tmol a^{-1} east of the dateline between 10°S and 10°N (implying an average rate of only about 0.2 mol m^{-2} a^{-1}) is in line with the model estimate of *Jiang et al.* [2003] but are threefold lower than the modeled estimates of *Gnanadesikan* [1999] and six- to eight-fold lower than the modeled estimates of *Heinze et al.* [2003]. This discrepancy suggests that either the satellite-based estimates of POC flux are too low or that both of the models used by *Gnanadesikan* [1999] and *Heinze et al.* [2003] have excessive tropical upwelling. We suggest this issue as a focus for future modeling experiments.

[40] We provide a more detailed analysis of variability in Figure 8. Variability in monthly particle export (standard deviation of monthly values over the 1998–2004 period divided by the mean over the 1998–2004 period multiplied by 100) is shown in Figure 8a. This treatment of variability illustrates the high month-to-month variability in polar regions as expected because of the solar cycle but also some high areas of variability in the tropical Atlantic and tropical Indian oceans and the subpolar frontal regions but relatively low variability in the equatorial Pacific. Much of the overall variability is diminished when data are averaged over the annual cycle (standard deviation of annually averaged values over the 1998–2004 period divided by the mean over the 1998–2004 period multiplied by 100), as shown in Figure 8b. The great exception to this is along the Antarctic coastline where two- to three-fold variations in annual particle export are seen from year to year. However, it is not clear how much of the variability is real as some of it may be due to aliasing because of poor satellite coverage due to clouds. Further analysis of annual versus interannual timescales of variability (standard deviation of annually averaged values over the 1998–2004 period divided by the standard deviation of monthly values over the 1998–2004 period multiplied by 100; Figure 8c) demonstrates that globally the seasonal variability in particle export dwarfs the interannual variability, with interannual variability accounting for only about 10–30% of the total variance in most regions. The one exception to this general trend is the central tropical Pacific, where interannual variability accounts for 50–70% of the monthly averaged particle export variability.

[41] This analysis provides a fascinating look at the nature of particle export variability. It suggests that most variability in particle export relative to the mean state occurs in polar, coastal and gyre boundary regions (Figure 8a), but that only in the ice-influenced Southern Ocean does year to year variability in total export vary more than 30% (Figure 8b). Still, in all subpolar and polar regions, it suggests that intra-annual variability swamps interannual variability overall, with the only areas with strong interannual variability being the equatorial Pacific and the subtropical gyres of the Atlantic and Indian oceans.

4.2. Penetration of Export Flux to Deep-Sea Sediments

[42] In representing observed vertical gradients in POC fluxes, the *Martin et al.* [1987] function provides a critical improvement over exponential decay in that it guarantees that a certain fraction of surface production penetrates through the water column to the seafloor. The *Klaas and Archer* [2002] treatment quantifies a mechanistic explanation for this functionality, arguing that POC does not penetrate through the water column unless it is protected by mineral, similar to but importantly different than arguments made by *Armstrong et al.* [2002] and *Francois et al.* [2002]. Whether this protection mechanism is through the increase in sinking velocity via ballasting or through a decrease in the remineralization rate constant via biological unavailability is still an open question. Because the protected portion can be regionally larger or smaller than that assumed in the Martin curve depending on SiO_2, $CaCO_3$ or lithogenic export, it provides a means through which the biogenic cycles of the elements are coupled.

[43] Our analysis of the satellite-derived export estimates and comparison with benthic oxygen utilization and sediment POC burial estimates demonstrates a surprisingly strong level of internal consistency between these approaches given the uncertainties involved. Because this internal consistency was only achievable through the application of the full mineral protection model of particle flux penetration including protection by $CaCO_3$, SiO_2 and lithogenic components, our analysis provides a new line of support for the theory of mineral protection of POC as a means of transporting it to the deep sea in accounting for regional variability in flux penetration length scales. Furthermore, the comparison between lithogenic fluxes through atmospheric deposition and sediment burial demonstrates the importance of both atmospherically and riverine derived lithogenic material in POC cycling. *Klaas and Archer* [2002] estimated the protection of organic material flux to the seafloor below 1000 m to be dominated by $CaCO_3$ almost exclusively, with $CaCO_3$ accounting for 80–83% of mineral protection, followed by SiO_2 (11–15%) and lithogenic material (clay; 5–6%). Our analysis suggests that lithogenic material plays a much larger role than previously considered, with $CaCO_3$ still accounting for a majority (56%; sensitivity range 42–76%) of mineral protection but with lithogenic material (38%; sensitivity range 16–51%) following close behind and SiO_2 (6%) falling a distant third. This result suggests that models which exclude the role of lithogenic material will significantly underestimate the penetration of POC to the deep seafloor by approximately 38% globally, and by a much larger fraction in areas with low productivity. However, a great deal of uncertainty remains in both lithogenic fluxes in particular and the regional variability in mass accumulation in sediments as a whole. We consider this topic to be in great need of further, focused observational and synthesis work.

4.3. Role of the Nearshore Environment in Carbon Burial

[44] One particularly surprising result of our analysis was the very high value for carbon burial (0.48 Pg C a^{-1}) in

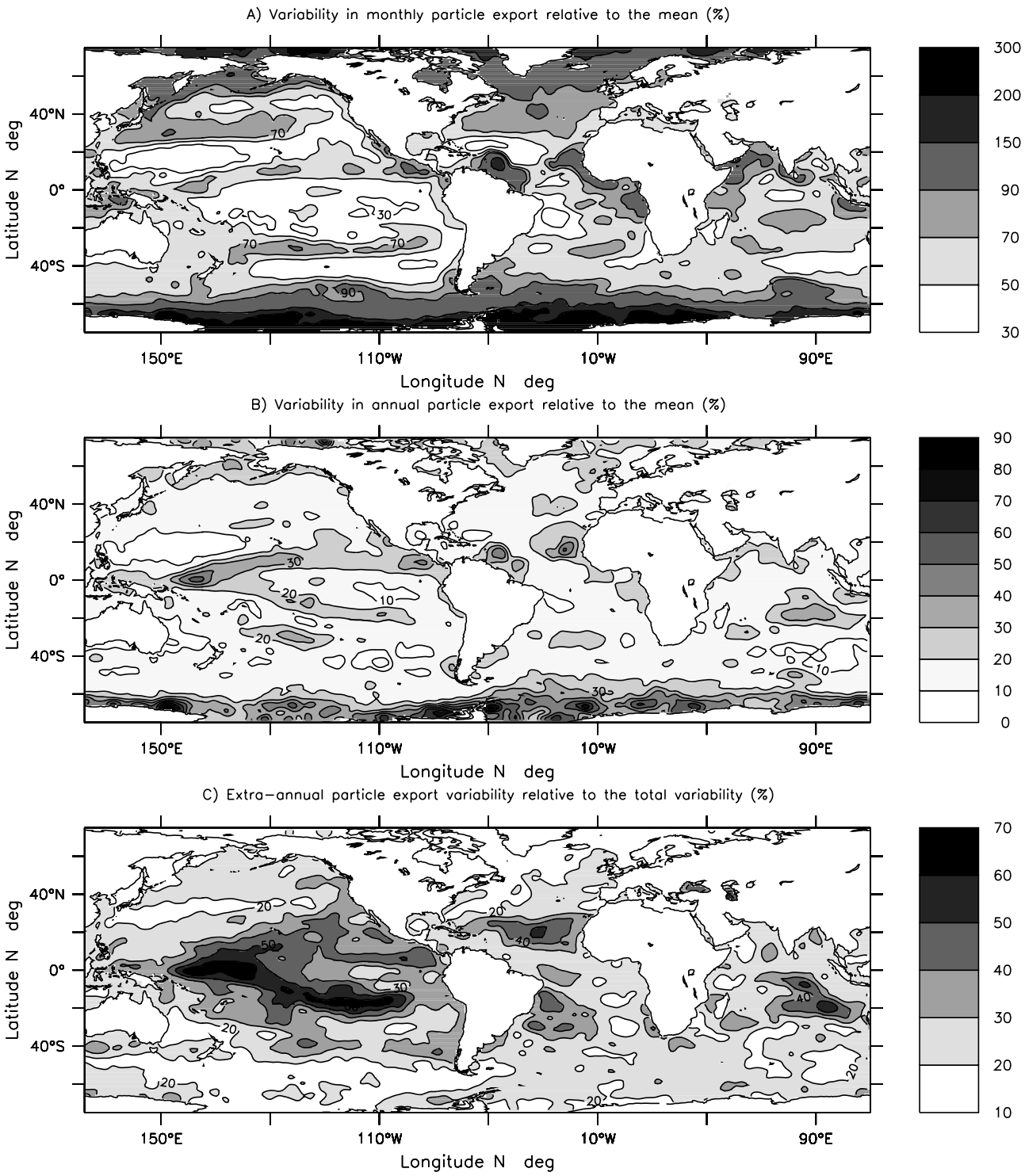

Figure 8. Global ocean particulate organic carbon export (PE) variability in terms of percent relative standard deviation. (a) Variation in monthly particle export relative to the mean ($\sigma_{PE}/PE_{ave} \times 100$). (b) Variation in annual particle export relative to the mean ($\sigma_{ann.ave.PE}/PE_{Ave} \times 100$). (c) Extra-annual variation relative to the total monthly particle export variability ($\sigma_{ann.ave.PE}/\sigma_{PE} \times 100$).

waters less than 50 m depth. This number is significantly higher than the global organic carbon burial estimate of 0.12–0.25 Pg C a^{-1} from *Hedges and Keil* [1995]. This large value is fundamentally driven by the strong relationship between carbon flux and carbon burial from primarily deeper environments used in our algorithms. Because this algorithm ignores sediment transport processes which tend to erode these physically dynamic, shallow regions in favor

of accumulation in deeper regions, we suspect that this estimate might better reflect the initial POC supply to sediments rather than the permanent in situ burial. Whether indicative of burial, in situ oxygen demand or enhanced sediment transport into slope regions, we suggest that our high values of POC supply to nearshore sediments highlight another area in clear need of further research.

5. Conclusions

[45] This paper has presented a new set of estimates for biogenic cycling in the oceans. When compared with the output of numerical models, the results suggest that a consensus view on the magnitude of global particulate organic carbon (POC) cycling is emerging. Our results suggest that a majority of POC burial occurs in relatively shallow waters. The dramatic importance of the nearshore and shelf regions to the permanent burial of carbon and the vast uncertainty in this estimate necessitates further work to understand carbon cycling in these complex nearshore and shelf regions. Overall, interannual variability was found to be relatively small, with the exception of El Niño–associated variability in the central tropical Pacific. Our comparison with sediment derived organic carbon and lithogenic material fluxes provide a new line of support for the mineral protection theory of POC flux and regional variability in penetration length scales. While previous studies included only atmospherically derived dust, this study demonstrates the critical role of river-derived lithogenic material as a potentially important carrier phase of POC to the seafloor.

[46] **Acknowledgments.** The authors would like to thank the SeaWiFS Project (code 970.2) and the Distributed Active Archive Center (code 902) at the Goddard Space Flight Center, Greenbelt, MD 20771, for the production and distribution, respectively, of these data. These activities are sponsored by NASA's Mission to Planet Earth Program. We would also like to thank Maureen Kennelly for assistance with processing SeaWiFS data, the NOAA-NCAR-NCEP reanalysis program for providing irradiance and surface temperature fields, and Mike Behrenfeld, Mary-Elena Carr, and John Marra for providing their primary production algorithms. Matthias Zabel, Richard Jahnke, and David Archer kindly provided data analyses from their published works. Eric Galbraith and Robbie Toggweiler provided helpful criticism. This work was supported by the Department of Commerce (JPD, AG) the DOE Ocean Carbon Sequestration Initiative, DOE grant FG0200ER63009 (JPD, JLS), and NASA Earth Science Enterprise Modeling, Analysis and Prediction grant NNG06GE77G (JLS).

References

Anderson, L. A., and J. L. Sarmiento (1994), Redfield ratios of remineralization determined by nutrient data analysis, *Global Biogeochem. Cycles*, *8*, 65–80.

Armstrong, R. A., C. Lee, J. I. Hedges, S. Honjo, and S. G. Wakeham (2002), A new, mechanistic model for organic carbon fluxes in the ocean based on the quantitative association of POC with ballast minerals, *Deep Sea. Res., Part II*, *49*, 219–236.

Aumont, O., E. Maier-Reimer, S. Blain, and P. Monfray (2003), An ecosystem model of the global ocean including Fe, Si, P colimitations, *Global Biogeochem. Cycles*, *17*(2), 1060, doi:10.1029/2001GB001745.

Behrenfeld, M. J., and P. G. Falkowski (1997), Photosynthetic rates derived from satellite-based chlorophyll concentration, *Limnol. Oceanogr.*, *42*, 1–20.

Berelson, W. M. (2002), Particle sinking rates increase with depth in the ocean, *Deep Sea Res., Part II*, *49*, 237–251.

Berelson, W. M., et al. (1997), Biogenic budgets of particle rain, benthic remineralization and sediment accumulation in the equatorial Pacific, *Deep Sea Res., Part II*, *44*, 2251–2282.

Berelson, W. M., W. M. Balch, R. Najjar, R. A. Feely, C. Sabine, and K. Lee (2007), Relating estimates of $CaCO_3$ production, export, and dissolution in the water column to measurements of $CaCO_3$ rain into sediment traps and dissolution on the sea floor: A revised global carbonate budget, *Global Biogeochem. Cycles*, *21*, GB1024, doi:10.1029/2006GB002803.

Berger, W. (1989), Global maps of ocean productivity, in *Productivity of the Ocean: Present and Past*, edited by W. H. Berger, V. S. Smetacek, and G. Wefer, pp. 429–455, John Wiley, New York.

Burdige, D. J., W. M. Berelson, K. H. Coale, J. McManus, and K. S. Johnson (1999), Fluxes of dissolved organic carbon from California continental margin sediments, *Geochim. Cosmochim. Acta*, *63*, 1507–1515.

Campbell, J., et al. (2003), Comparison of algorithms for estimating ocean primary production from surface chlorophyll, temperature, and irradiance, *Global Biogeochem. Cycles*, *16*(3), 1035, doi:10.1029/2001GB001444.

Canfield, D. E. (1993), Organic matter oxidation in marine sediments, in *Interactions of C, N, P and S Biogeochemical Cycles and Global Change*, *NATO ASI Ser.*, vol. 14, edited by R. Wollast, L. Chou, and F. Mackensie, pp. 333–363, Springer-Verlag, Berlin.

Canfield, D. E. (1994), Factors influencing organic carbon preservation in marine sediments, *Chem. Geol.*, *114*, 315–329.

Carr, M.-E. (2002), Estimation of potential productivity in Eastern Boundary Currents using remote sensing, *Deep Sea Res., Part II*, *49*, 59–80.

Carr, M.-E., et al. (2006), A comparison of global estimates of primary production from ocean color, *Deep Sea Res., Part II*, *53*, 741–770.

Chung, S.-N., K. Lee, R. A. Feely, C. L. Sabine, F. J. Millero, R. Wanninkhof, J. L. Bullister, R. M. Key, and T.-H. Peng (2003), Calcium carbonate budget in the Atlantic Ocean based on water column inorganic carbon chemistry, *Global Biogeochem. Cycles*, *17*(4), 1093, doi:10.1029/2002GB002001.

DeMaster, D. J. (2002), The accumulation and cycling of biogenic silica in the Southern Ocean: Revisiting the marine silica budget, *Deep Sea Res., Part II*, *49*, 3155–3167.

Dunne, J. P., J. W. Murray, A. K. Aufdenkampe, S. Blain, and M. Rodier (1999), Silicon:nitrogen coupling in the equatorial Pacific upwelling zone, *Global Biogeochem. Cycles*, *13*, 715–726.

Dunne, J. P., R. A. Armstrong, A. Gnanadesikan, and J. L. Sarmiento (2005), Empirical and mechanistic models for the particle export ratio, *Global Biogeochem. Cycles*, *19*, GB4026, doi:10.1029/2004GB002390.

Feely, R. A., et al. (2002), In situ calcium carbonate dissolution in the Pacific Ocean, *Global Biogeochem. Cycles*, *16*(4), 1144, doi:10.1029/2002GB001866.

Feldman, G., et al. (1989), Ocean color: Availability of the global data set, *Eos Trans. AGU*, *70*, 634–641.

Francois, R., S. Honjo, R. Krishfield, and S. Manganini (2002), Factors controlling the flux of organic carbon to the bathypelagic zone of the ocean, *Global Biogeochem. Cycles*, *16*(4), 1087, doi:10.1029/2001GB001722.

Friis, K., R. G. Najjar, M. J. Follows, and S. Dutkiewicz (2006), Possible overestimation of shallow-depth calcium carbonate dissolution in the ocean, *Global Biogeochem. Cycles*, *20*, GB4019, doi:10.1029/2006GB002727.

Ganachaud, A., and C. Wunsch (2002), Oceanic nutrient and oxygen transports and bounds on export production during the World Ocean Circulation Experiment, *Global Biogeochem. Cycles*, *16*(4), 1057, doi:10.1029/2000GB001333.

Gao, Y., S.-M. Fan, and J. Sarmiento (2003), Aeolian iron input to the ocean through precipitation scavenging: A modeling perspective and its implication for natural iron fertilization in the ocean, *J. Geophys. Res.*, *108*(D7), 4221, doi:10.1029/2002JD002420.

Gent, P. R., and J. C. McWilliams (1990), Isopycnal mixing in ocean circulation models, *J. Phys. Oceanogr.*, *20*, 150–155.

Ginoux, P., M. Chin, I. Tegen, J. M. Prospero, B. Holben, O. Dubovik, and S.-J. Lin (2001), Sources and distributions of dust aerosols simulated with the GOCART model, *J. Geophys. Res.*, *106*, 20,255–20,273.

Gnanadesikan, A. (1999), A global model of silicon cycling: Sensitivity to eddy parameterization and dissolution, *Global Biogeochem. Cycles*, *13*, 199–220.

Gnanadesikan, A., and J. R. Toggweiler (1999), Constraints placed by silicon cycling on vertical exchange in general circulation models, *Geophys. Res. Lett.*, *26*, 1865–1868.

Gnanadesikan, A., R. D. Slater, N. Gruber, and J. L. Sarmiento (2002), Oceanic vertical exchange and new production: A comparison between models and observations, *Deep Sea Res., Part II*, *49*, 363–401.

Gnanadesikan, A., J. P. Dunne, R. M. Key, K. Matsumoto, J. L. Sarmiento, R. D. Slater, and P. S. Swathi (2004), Oceanic ventilation and biogeochemical cycling: Understanding the physical mechanisms that produce realistic distributions of tracers and productivity, *Global Biogeochem. Cycles*, *18*, GB4010, doi:10.1029/2003GB002097.

Gregg, W. W., M. E. Conkright, J. E. O'Reilly, F. S. Patt, M. H. H. Wang, J. A. Yoder, and M. W. Casey (2002), The NOAA-NASA Coastal Zone Color Scanner reanalysis effort, *Ocean Optics*, *41*, 1615–1628.

Hansell, D. A., and C. A. Carlson (1998), Net community production of dissolved organic carbon, *Global Biogeochem. Cycles*, *12*, 443–453.

Hartnett, H. E., and A. H. Devol (2003), Role of a strong oxygen deficient zone in the preservation and degradation of organic matter: A carbon budget for the continental margins of NW Mexico and Washington State, *Geochim. Cosmochim. Acta*, *67*, 247–264.

Hedges, J. H., and R. Keil (1995), Sedimentary organic matter preservation: An assessment and speculative synthesis, *Mar. Chem.*, *49*, 81–115.

Heinze, C., E. Maier-Reimer, A. M. E. Winguth, and D. A. Archer (1999), A global sediment model for long-term climate studies, *Global Biogeochem. Cycles*, *13*, 221–250.

Heinze, C., A. Hupe, E. Maier-Reimer, N. Dittert, and O. Ragueneau (2003), Sensitivity of the marine biospheric Si cycle for biogeochemical parameter variations, *Global Biogeochem. Cycles*, *17*(3), 1086, doi:10.1029/2002GB001943.

Jahnke, R. A. (1996), The global ocean flux of particulate organic carbon: Areal distribution and magnitude, *Global Biogeochem. Cycles*, *10*, 71–88.

Jiang, M. S., F. Chai, R. C. Dugdale, F. P. Wilkerson, T. H. Peng, and R. T. Barber (2003), A nitrate and silicate budget in the equatorial Pacific Ocean: A coupled physical-biological model study, *Deep Sea Res., Part II*, *50*, 2971–2996.

Jin, X., N. Gruber, J. P. Dunne, J. L. Sarmiento, and R. A. Armstrong (2006), Diagnosing the contribution of phytoplankton functional groups to the production and export of particulate organic carbon, $CaCO_3$, and opal from global nutrient and alkalinity distributions, *Global Biogeochem. Cycles*, *20*, GB2015, doi:10.1029/2005GB002532.

Kalnay, E., et al. (1996), The NCEP/NCAR 40-year reanalysis project, *Bull. Am. Meteorol. Soc.*, *77*, 437–471.

Klaas, C., and D. Archer (2002), Association of sinking organic matter with various types of mineral ballast in the deep sea: Implications for the rain ratio, *Global Biogeochem. Cycles*, *16*(4), 1116, doi:10.1029/2001GB001765.

Laws, E. A., P. Falkowski, W. O. Smith, H. Ducklow, and J. J. McCarthy (2000), Temperature effects on export production in the open ocean, *Global Biogeochem. Cycles*, *14*, 1231–1246.

Lee, K. (2001), Global net community production estimated from the annual cycle of surface water total dissolved inorganic carbon, *Limnol. Oceanogr.*, *46*, 1287–1297.

Lee, K., L. T. Tong, F. J. Millero, C. L. Sabine, A. G. Dickson, C. Goyet, G.-H. Park, R. Wanninkof, R. A. Feely, and R. M. Key (2006), Global relationships of total alkalinity with salinity and temperature in surface waters of the world's oceans, *Geophys. Res. Lett.*, *33*, L19605, doi:10.1029/2006GL027207.

Lutz, M., R. Dunbar, and K. Caldiera (2002), Regional variability in the vertical flux of particulate organic carbon in the ocean interior, *Global Biogeochem. Cycles*, *16*(3), 1037, doi:10.1029/2000GB001383.

Marra, J., C. Ho, and C. C. Trees (2003), An alternative algorithm for the calculation of primary productivity from remote sensing data, *LDEO Tech. Rep. LDEO-2003-1*, Lamont Doherty Earth Obs., Palisades, N. Y.

Martin, J. H., G. A. Knauer, D. M. Karl, and W. W. Broenkow (1987), VERTEX: Carbon cycling in the northeastern Pacific, *Deep Sea Res., Part I*, *34*, 267–285.

Milliman, J. D., and P. J. Troy (1999), Biologically mediated dissolution of calcium carbonate above the chemical lysocline?, *Deep Sea Res., Part I*, *46*, 1653–1670.

Moore, J. K., S. C. Doney, and K. Lindsay (2004), Upper ocean ecosystem dynamics and iron cycling in a global three-dimensional model, *Global Biogeochem. Cycles*, *18*, GB4028, doi:10.1029/2004GB002220.

Muller-Karger, F. E., R. Varela, R. Thunell, R. Luerssen, C. Hu, and J. J. Walsh (2004), The importance of continental margins in the global carbon cycle, *Geophys. Res. Lett.*, *32*, L01602, doi:10.1029/2004GL021346.

Najjar, R., and J. C. Orr (1998), Design of OCMIP-2 simulations of chlorofluorocarbons, the solubility pump and common biogeochemistry, internal OCMIP report, 25 pp., LSCE/CEA Saclay, Gif-sur-Yvette, France.

Nelson, D. M., P. Treguer, M. A. Brzezinski, A. Leynaert, and B. Queguiner (1995), Production and dissolution of biogenic silica in the ocean: Revised global estimates, comparison with regional data and relationship to biogenic sedimentation, *Global Biogeochem. Cycles*, *9*, 359–372.

Nelson, D. M., et al. (2002), Vertical budgets for organic carbon and biogenic silica in the Pacific sector of the Southern Ocean, 1996–1998, *Deep Sea Res., Part II*, *49*, 1645–1674.

Papadimitriou, S., H. Kennedy, I. Bentaleb, and D. N. Thomas (2002), Dissolved organic carbon in sediments from the eastern North Atlantic, *Mar. Chem.*, *79*, 37–47.

Platt, T. (1986), Primary production of the ocean water column as a function of surface light intensity: Algorithms for remote sensing, *Deep Sea Res., Part A*, *33*, 149–163.

Pollard, R. M., P. Treguer, and J. Read (2006), Quantifying nutrient supply to the Southern Ocean, *J. Geophys. Res.*, *111*, C05011, doi:10.1029/2005JC003076.

Pondaven, P., O. Ragueneau, P. Treguer, A. Hauvespre, L. Dezileau, and J. L. Reyss (2000), Resolving the "opal paradox" in the Southern Ocean, *Nature*, *405*, 168–172.

Ryther, J. H., and C. S. Yentsch (1957), The estimation of phytoplankton production in the ocean from chlorophyll and light data, *Limnol. Oceanogr.*, *2*, 281–286.

Sabine, C. L., R. M. Key, R. A. Feely, and D. Greeley (2002), Inorganic carbon in the Indian Ocean: Distribution and dissolution processes, *Global Biogeochem. Cycles*, *16*(4), 1067, doi:10.1029/2002GB001869.

Sarmiento, J. L., J. Dunne, A. Gnanadesikan, R. M. Key, K. Matsumoto, and R. Slater (2002), A new estimate of the $CaCO_3$ to organic carbon export ratio, *Global Biogeochem. Cycles*, *16*(4), 1107, doi:10.1029/2002GB001919.

Sarmiento, J. L., N. Gruber, M. Brzezinski, and J. P. Dunne (2004), High-latitude controls of thermocline nutrients and low latitude biological productivity, *Nature*, *427*, 56–60.

Sayles, F. L., W. R. Martin, Z. Chase, and R. F. Anderson (2001), Benthic remineralization and burial of biogenic SiO_2, $CaCO_3$, organic carbon, and detrital material in the Southern Ocean along a transect at 170° west, *Deep Sea Res., Part II*, *48*, 4323–4383.

Schlitzer, R. (2004), Export production in the North Pacific derived from dissolved oxygen, nutrient, and carbon data, *J. Oceanogr.*, *60*, 53–62.

Seiter, K., C. Hensen, E. Schroter, and M. Zabel (2004), Organic carbon content in surface sediments- defining regional provinces, *Deep Sea Res., Part I*, *51*, 2001–2026.

Sokal, R. R., and F. J. Rohlf (1995), *Biometry: The Principles and Practice of Statistics in Biological Research*, 3rd ed., 887 pp., W. H. Freeman, New York.

Treguer, P., D. M. Nelson, A. J. Van Bennekom, D. J. DeMaster, A. Leynaert, and B. Quguiner (1995), The silica balance in the world ocean: A reestimate, *Science*, *268*, 375–379.

J. P. Dunne and A. Gnanadesikan, NOAA Geophysical Fluid Dynamics Laboratory, P.O. Box 308, Princeton, NJ 08542, USA. (john.dunne@noaa.gov; anand.gnanadesikan@noaa.gov)

J. L. Sarmiento, AOS Program, Princeton University, P.O. Box CN710, Princeton, NJ 08544, USA. (jls@princeton.edu)